ACS Chemical Neuroscience
Cite This: ACS Chem. Neurosci. 2019, 10, 1524−1534
Research Article
pubs.acs.org/chemneuro

Impact on Glioblastoma U87 Cell Gene Expression of a Carborane Cluster-Bearing Amino Acid: Implications for Carborane Toxicity in Mammalian Cells

Tianyu He,[†] Sridar V. Chittur,[‡] and Rabi A. Musah*,[†]

[†]Department of Chemistry, University at Albany, State University of New York, 1400 Washington Avenue, Albany, New York 12222, United States

[‡]Center for Functional Genomics, University at Albany, State University of New York, 1 Discovery Drive, Rensselaer, New York 12144, United States

Supporting Information

ABSTRACT: Carboranes have been extensively investigated as potential drugs for the treatment of malignant human brain tumors by boron neutron capture therapy (BNCT). This noninvasive treatment modality utilizes compounds containing the nonradioactive isotope ^{10}B which has a high propensity to capture slow neutrons. In response, it emits high energy α-particles that kill the cell. We have successfully synthesized a boron delivery agent by installing a boron-rich *m*-carborane within the amino acid cysteine. Rapid uptake of this compound into U87 glioblastoma cells within 5 min of exposure was observed, and fluorescence microscopy studies showed that it was retained intracellularly after 48 h. In the absence of thermal neutrons, a cytostatic effect in U87 cells was observed at exposures ranging from 1 μM to 1 mM relative to the control, while no change was observed at 1−0.01 μM. Microarray studies unveiled a wide range of unique changes in the gene expression profile of the U87 cells, particularly for the genes associated with cell cycle, which were observed to be greatly suppressed after treatment with the compound. These results were validated by qPCR studies. Although the compound was designed for BNCT, its distinctive impacts on gene regulation reveal that it and other carborane-containing cluster molecules may exert unique heretofore unknown effects on the transcriptome, even in the absence of applied radiation.

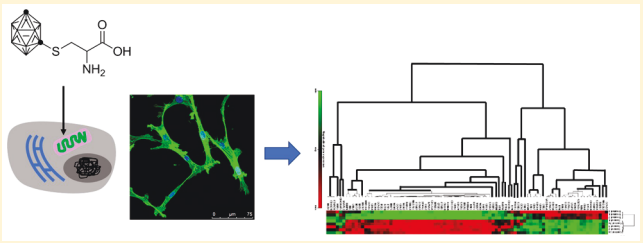

KEYWORDS: *Carborane, unnatural amino acid, boron delivery, cell cycle, cytostatic, apoptosis*

INTRODUCTION

While the element boron is an essential trace mineral in living systems, it is unusual to observe it in plant and animal cells in a form that is integrated into organic molecules through covalent bonding with carbon. Nevertheless, by virtue of a number of unique properties, organoboranes are perceived to hold significant promise as therapeutic agents. There have been numerous investigations of the medicinal chemistry of organoboranes, although only one boron-containing drug bortezomib (marketed as Velcade) has been approved by the United States Food and Drug Administration for treatment of multiple myeloma.[1]

Natural abundance boron is composed primarily of ^{10}B (~20%) and ^{11}B (~80%). One of the attributes of the ^{10}B isotope in particular, is its nuclear fission when irradiated with thermal neutrons, which ultimately results in the production of ^{7}Li nuclei and α-particles. This characteristic of ^{10}B has been exploited for the development of boron neutron capture therapy (BNCT), which refers to a two-step cancer treatment sequence involving: (1) uptake by tumor cells of a boron-containing molecule; and (2) killing of the cancer cells through the action of the α-particles produced by irradiation of the tumor. Since the trajectory of the resulting particles is 5−9 μm, which approximates the diameter of a single cell, radiation damage is by and large limited to the cells which contain the boron delivery agent. Thus, in principle, the side-effects of conventional ionizing radiation therapy can be avoided, providing there is selective uptake of the boron delivery agent by the targeted tumor cells. Several boron-containing amino acids have been evaluated as boron delivery agents, and their cell killing effects in mice has been reported.[2−5] These include boronophenylalanine (BPA) and other unnatural boron-containing amino acids like those containing borocaptate.[3,6] These compounds are characterized by having a single boron atom per molecule. However, because only 20% of boron is ^{10}B, the uptake into cancer cells of boron-rich payloads is perceived to be the most viable mechanism by which to generate enough α-particle-induced radiation to effect significant tumor damage. For this reason, boron cluster compounds that contain multiple boron atoms per molecule

Received: September 26, 2018
Accepted: November 26, 2018
Published: November 26, 2018

DOI: 10.1021/acschemneuro.8b00512
ACS Chem. Neurosci. 2019, 10, 1524−1534

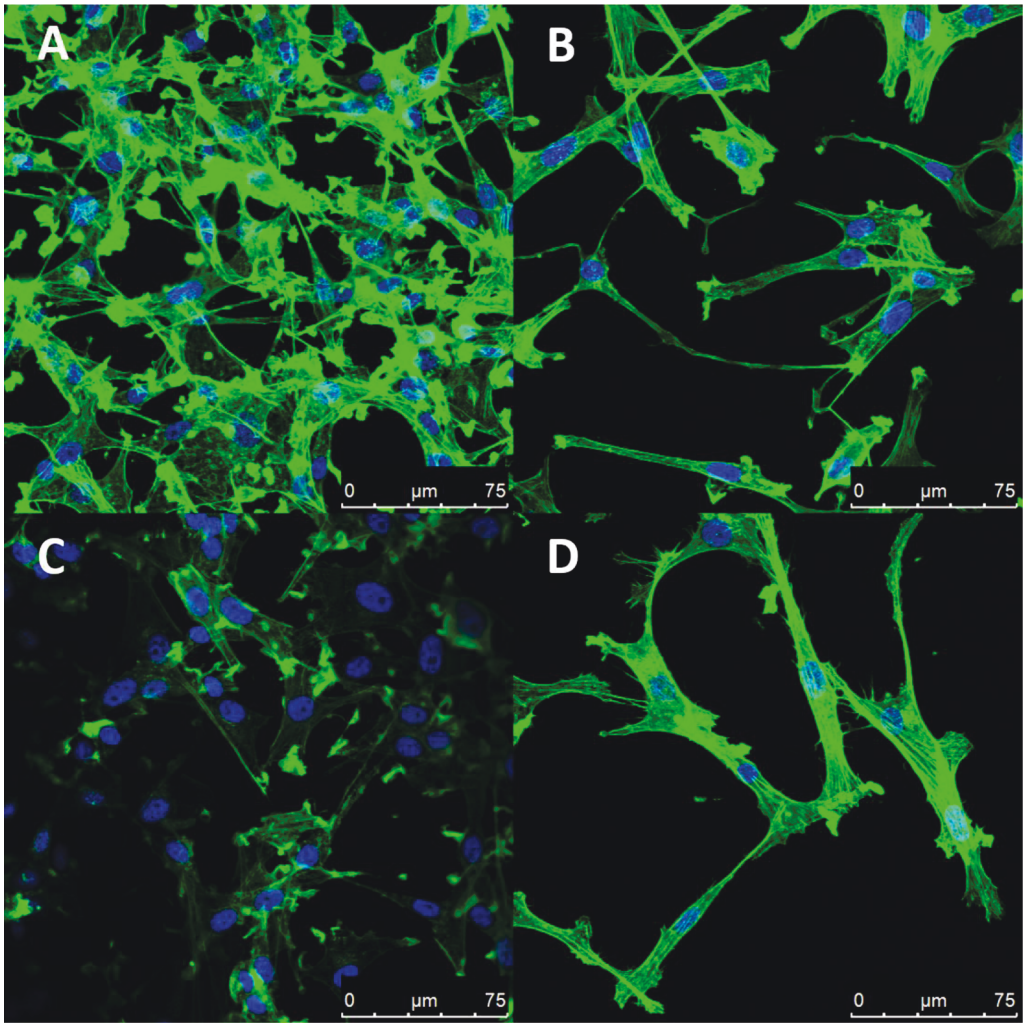

Figure 1. U87 cell morphological changes induced by exposure to 1 mM of compound **3**. (A) Untreated U87 cells after 24 h. (B) Exposure of the U87 cells to 1 mM compound **3** resulted in morphological changes marked by cell elongation. (C) Untreated U87 cells after 48 h. The cells retained the morphology of the untreated control and were at a higher density. (D) After 48 h of exposure to 1 mM of compound **3**, the morphological changes were retained and the cell population remained identical to that at the start of the experiment, indicating a cytostatic effect.

such as boranes and carboranes, have featured prominently in the development of potential BNCT agents. While the boranes are polyhedra comprised of boron and hydrogen only, the carboranes contain boron, carbon and hydrogen atoms. Like many of the boranes, these carboranes are polyhedral and are classified as *closo-*, *nido-*, *arachno-*, *hypho-*, etc., based on whether they represent a complete (*closo-*) polyhedron, or a polyhedron that is missing one (*nido-*), two (*arachno-*), or more vertices. It has been suggested that the chemical inertness of polyhedral carboranes might render them suitable for a variety of therapeutic applications, and a number of cases have been reported in which the scaffold has been integrated into a larger structure that can potentially be used to treat disease.[7,8] Examples of such compounds that have been investigated as BNCT agents include sodium mercaptoundecahydro-*closo*-dodecaborate (BSH), and disodium-decahydro-*closo*-decaborate. These molecules are the only ones so far approved for human trials for treatment of the aggressive brain tumor glioblastoma multiforme.[7,9−14] To date, only limited success has been achieved using these compounds.[12,14−17] Challenges include poor bioavailability and limited tumor uptake.[18,19] Remarkably, while both in vitro and in vivo studies have been reported, there are no reports regarding the impact of these nonbiological borane and carborane clusters on the full gene expression profiles of the cells to which they are exposed.

In principle, the integration of carborane clusters within an architectural framework that mimics those common in nature, might enhance the biocompatibility and cell-entry characteristics of boron-rich compounds. Toward this goal, we have successfully synthesized 2-amino-3-(1,7-dicarba-*closo*-dodecaboranyl-1-thio)propanoic acid, a carborane-based amino acid whose design was inspired by the nonproteinogenic *S*-substituted cysteines utilized by plants of the *Allium* and other genera as plant chemical defense precursors.[20] We report here on the biological activity of this compound on the human glioblastoma cell line U87. The results show that the molecule undergoes rapid cellular uptake which is followed by dramatic changes in cell morphology. The effect of the molecule on U87 gene expression was investigated and represents the first report of the impact of a carborane cluster compound on the transcriptome. The carboranyl cysteine was observed to exert a dramatic effect on the gene expression profile of U87 cells and the results provide another possible context within which to view the potential effects of boron cluster compounds on mammalian cells.

DOI: 10.1021/acschemneuro.8b00512
ACS Chem. Neurosci. 2019, 10, 1524−1534

RESULTS AND DISCUSSION

2-Amino-3-(1,7-dicarba-*closo*-dodecaboranyl-1-thio)-propanoic Acid (3) Causes Dramatic Changes in the Morphology of U87 Cells. The investigation of the potential biological activity of **3** was initiated by monitoring its impact on immortalized human glioblastoma cells (U87). When U87 cells were exposed to EMEM media containing 1 mM of **3**, dramatic morphological changes were observed. This is illustrated in Figure 1, which shows a comparison of the morphology of untreated (panels A and C) and treated (panels B and D) cells that were fixed and double stained with phalloidin (an actin stain) and DAPI (a nuclear stain). In the absence of **3**, cells appeared as shown in panel A, and their morphology remained unchanged after 48 h (panel C). However, within 5 min of exposure to **3**, the cells adopted a spherical morphology, which was followed shortly thereafter by gradual elongation which was readily apparent at the 24 h time point (panel B). This change was maintained at 48 h (Panel D). Throughout the time course, the cells remained adherent.

To assess whether the observed morphological changes could be induced with other *S*-substituted cysteines, or if the effects were a unique consequence of the presence of the carborane cluster, the response of U87 cells to **3** was compared with that observed on exposure to four other *S*-substituted cysteine analogues in EMEM media at a concentration of 1 mM: *S*-allyl-L-cysteine (**1**); *S*-phenyl-L-cysteine (**2**); *S*-benzyl-L-cysteine (**4**); and *S*-phenylethyl-L-cysteine (**5**). The results, illustrated in Figure 2, showed that relative to the no-treatment control and with monitoring over a 48 h period, no morphological changes were apparent for *S*-substituted cysteines other than **3**. It was thus concluded that the carborane moiety was responsible for the unique effect of **3** on U87 cell morphology.

Carboranyl Cysteine 3 Crosses the U87 Cell Membrane. It has been suggested that an important attribute of an effective BNCT agent is that it be capable of crossing biological membranes.[21] This may be particularly important given that boron localized to the cell surface has been estimated to be 10% less effective at killing cells than an equimolar quantity of boron that is uniformly distributed throughout the cell.[21,22] To investigate whether **3** crosses the U87 cell membrane, advantage was taken of the observation that **3** exhibits fluorescence, with excitation and emission wavelengths of 320 and 423 nm, respectively (Supporting Information Figure S1). In order to obtain images in which the fluorescence response is readily apparent, we incubated the cells with 1 mM of **3**, which is the highest concentration achievable in an aqueous environment. Entry of **3** into U87 cells was monitored by tracking the change in fluorescence of the cells before and after exposure. Within 5 min of exposure, fluorescence was observed within the cell, which exhibited a higher intensity than the surrounding media (Supporting Information Figure S2, panel B). After 24 h, the compound was retained inside the cell, with a higher fluorescence intensity in the cytosol than in the nuclei. Furthermore, the cells adopted an elongated morphology (Figure S2, panel C). At 48 h post-treatment, the cells were further elongated when compared with the 24 h post-treatment and the compound was still retained in the cytosol with a lower fluorescence intensity in the nuclei compared with the 24 h post-treatment (Figure S2, panel D). The results demonstrated the rapid entry of compound **3** into U87 cells and retention of the compound within the cells after 48 h. Within 24 h, the distribution of the compound shifted from being concentrated in the nuclei to being more highly concentrated in the cytoplasm.

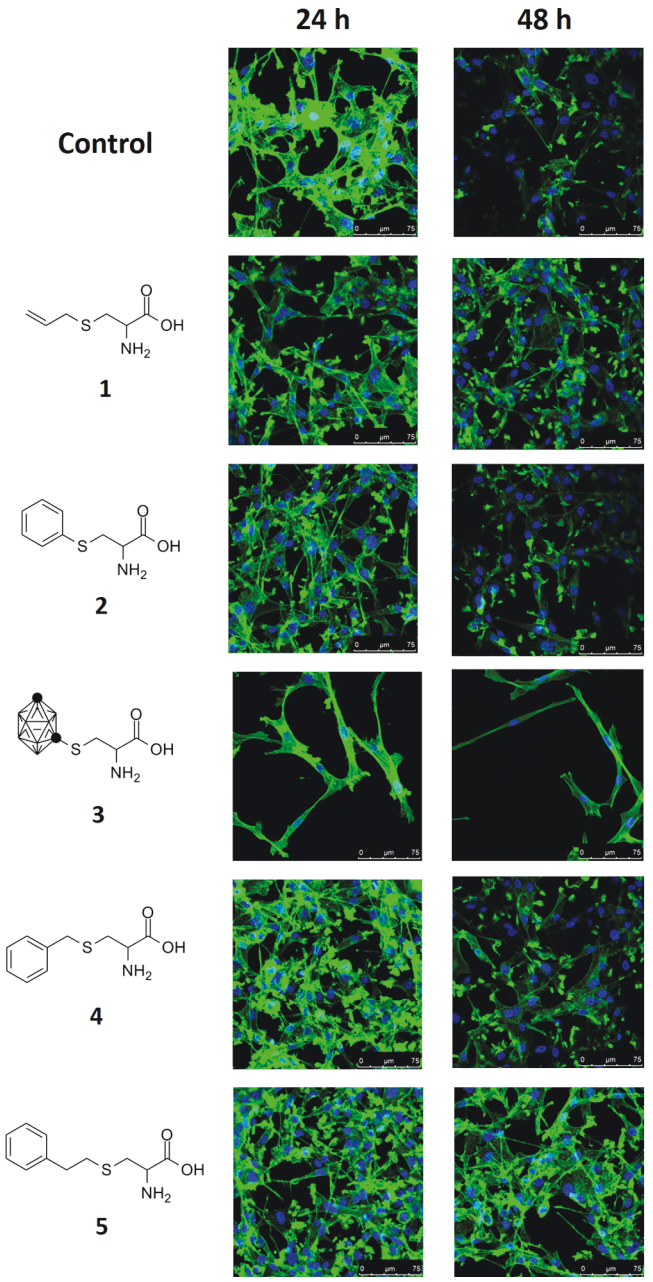

Figure 2. Exposure (24 and 48 h) of U87 cells to 1000 μM of various *S*-substituted cysteines. The U87 cells treated with compound **3** showed morphological changes marked by cell elongation. It also showed that the compound has a cytostatic effect on the U87 cells. However, treatment with other *S*-substituted cysteines showed retention of the morphology and similar cell densities to the control cells.

Carboranyl Cysteine 3 Exerts a Cytostatic Effect on U87 Cells. In order to determine the effect of **3** on cell viability, particularly when compared to that of other *S*-substituted-L-cysteines, U87 cell growth was monitored after exposure to compounds **1**−**5**. Cells were treated 48 h after being plated into 6-well plates, and the growth of the cells was monitored at 24 and 48 h post-treatment. The cell count and viability of each sample were determined in triplicate using a

DOI: 10.1021/acschemneuro.8b00512
ACS Chem. Neurosci. 2019, 10, 1524−1534

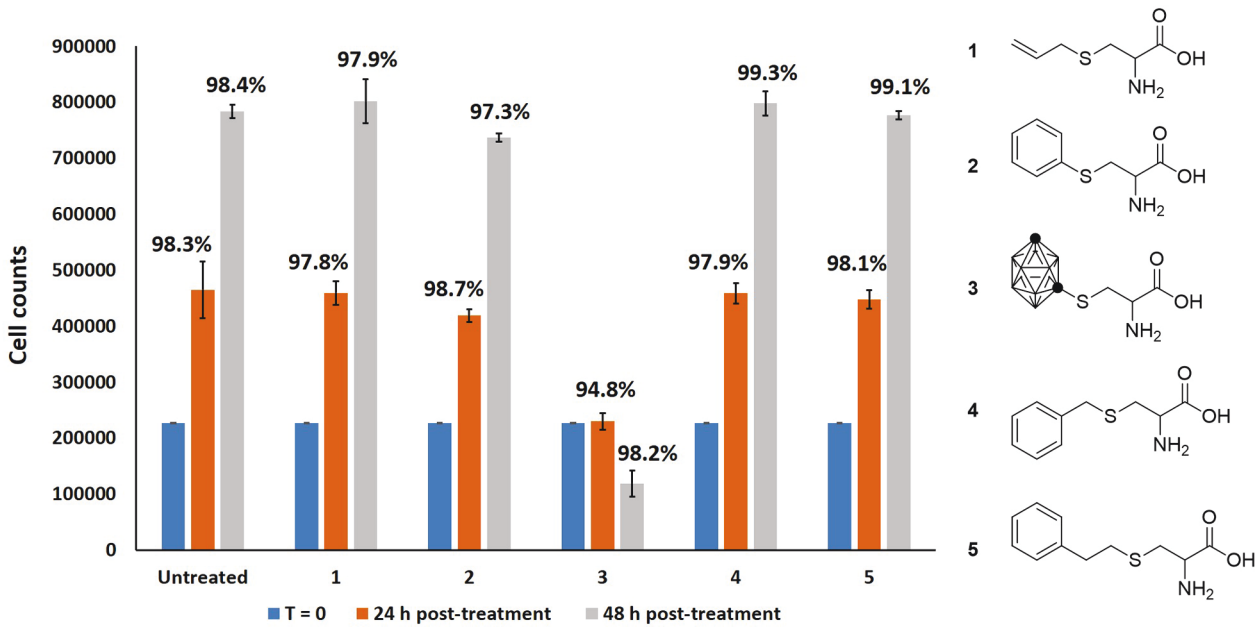

Figure 3. Effect of various *S*-substituted cysteines on U87 cells as a function of time. Cells at a density of 2.2×10^4 cells/cm^2 were treated with *S*-allyl cysteine (1), *S*-phenyl cysteine (2), *S*-carboranyl cysteine (3), *S*-benzyl cysteine (4), and *S*-phenylethyl cysteine (5). The control cells showed approximately 100% growth over 24 and 48 h. Cell growth on treatment with compounds **1**, **2**, **4**, and **5** was similar to that of the untreated control cells. Cells treated with compound **3** showed no growth after 24 h and a decrease in the cell population after 48 h. Blue, orange, and gray bars represent the cell counts at different time points (upon treatment, 24 h post-treatment, and 48 h post-treatment, respectively).

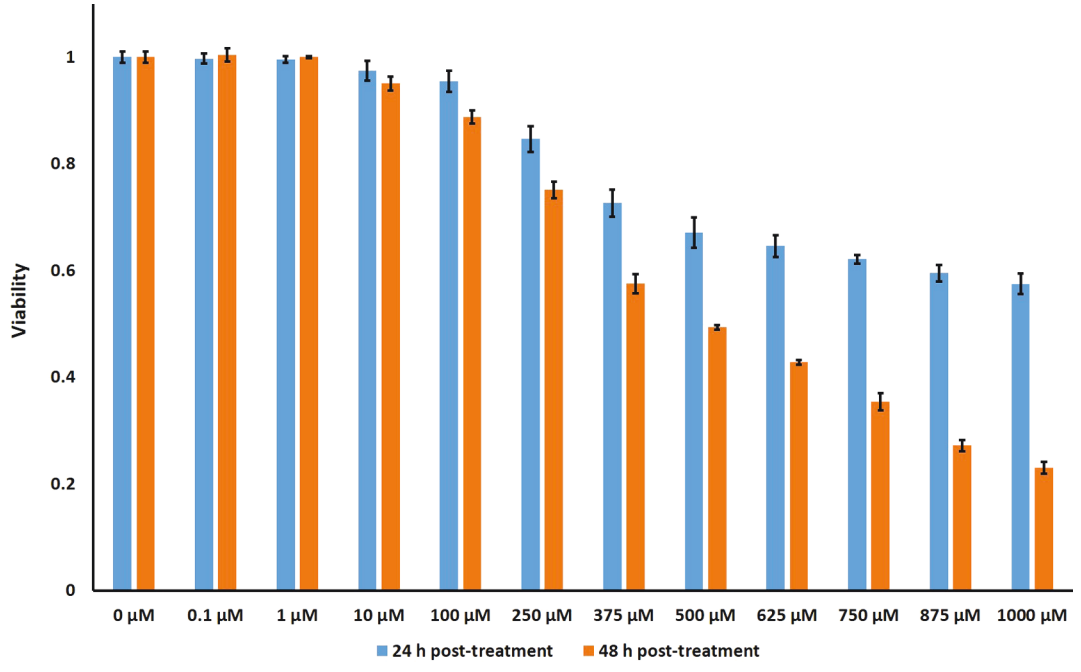

Figure 4. Response of U87 cells to compound **3** at various concentrations.

Muse cell analyzer. As illustrated in Figure 3, the cell counts for *S*-substituted cysteines other than **3** fell between 700,000 and 800,000 at 48 h post-treatment, and was approximately 450,000 at 24 h post-treatment, results which were similar to that of the control (i.e., ~780,000 at 48 h post-treatment and ~460,000 at 24 h post-treatment). In contrast, a cytostatic effect was observed in the cells treated with **3** at 24 h, and a 50% decrease in cell population was apparent at the 48 h time point. These findings were consistent with those observed in the cell imaging experiments whose results are presented in Figure 2, and indicate that the effect is a consequence of the presence in **3** of the carborane moiety.

Dose–Response Studies. Because the cell count experiments revealed a cytostatic effect on U87 cells on exposure to 1 mM compound **3**, dose response studies to determine the compound concentrations at which cell growth was affected were conducted. This was accomplished using the crystal violet assay. U87 cells were exposed to **3** at concentrations ranging from 0.1 μM to 1 mM, and the impacts at 24 and 48 h were determined. As demonstrated in Figure 4, compared to the

DOI: 10.1021/acschemneuro.8b00512
ACS Chem. Neurosci. 2019, 10, 1524–1534

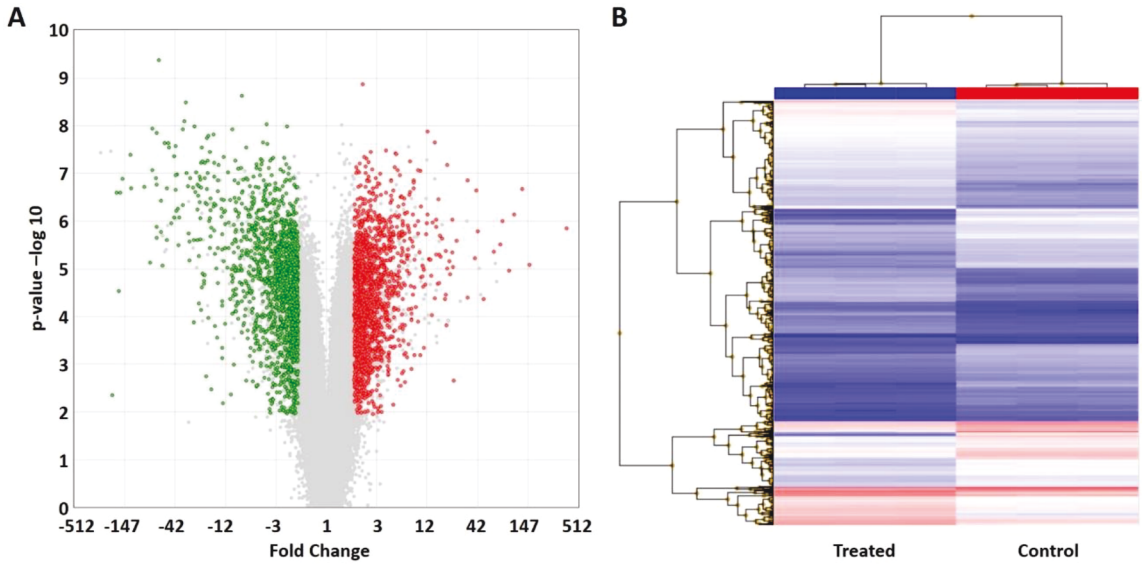

Figure 5. (A) "Volcano plot" showing differential gene expression (FC > 2, $p < 0.01$). The plot reflects the gene expression profile of over 3119 genes in response to exposure to compound **3** relative to nonexposed cells. The *x*-axis represents fold changes. Data points shown in green indicate downregulated genes and those in red indicate upregulated genes. Genes exhibiting less than a 2-fold change (FC) are shown in the gray-shaded area. (B) Hierarchical clustering analysis of differentially expressed genes in U87 cells after 48 h of treatment with compound **3**. Data are based on six individual and independent experiments. Columns represent subjects and rows represent genes. Blue indicates downregulated genes and red indicates upregulated genes.

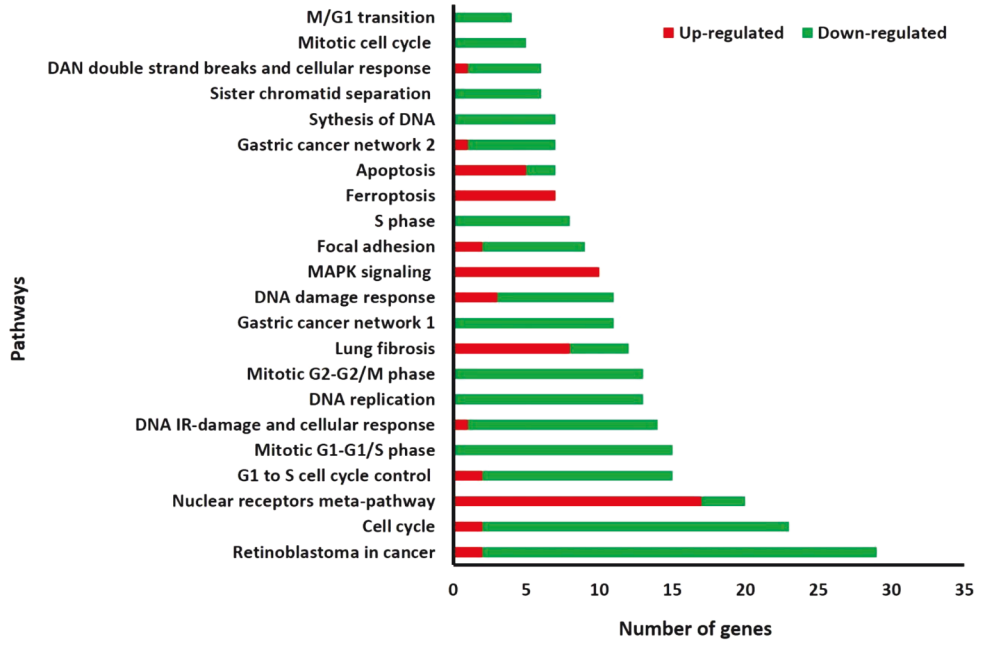

Figure 6. Biochemical pathways associated with differential gene expression (FC > 5, $p < 0.01$). Red and green bars indicate up- and downregulated genes, respectively. The *x*-axis represents the number of genes that were differentially expressed. The corresponding pathways are displayed on the *y*-axis.

control (0 μM), no changes in cell growth were observed from 0.1 to 1 μM. However, at higher concentrations, cell growth was gradually reduced, with a 33% and 51% reduction at 500 μM for the 24 and 48 h time points respectively, and a 43% and 77% reduction at 1 mM for the 24 and 48 h time points, respectively. The results demonstrated that with increasing concentrations of **3** above 100 μM, there was an increasing cytostatic effect at 24 h post-treatment and a cell killing effect by the 48 h time point. At concentrations lower than 100 μM, **3** demonstrated no evident toxicity in U87 cells.

Compound 3 Affects Gene Expression in U87 Cells.

To further investigate the effect of compound **3** on U87 cells, microarray analyses were conducted using the concentration of **3** that resulted in the most dramatic impact on cell viability. Cells were treated with 1 mM of **3** and the expression levels of genes were analyzed 48 h post-treatment using Affymetrix Human Transcriptome 2.0 ST arrays. Untreated cells were used as a control. From this analysis, 3119 coding genes were determined to be differentially expressed in response to treatment after 48 h, among which 1583 were upregulated

DOI: 10.1021/acschemneuro.8b00512
ACS Chem. Neurosci. 2019, 10, 1524−1534

Table 1. Differentially Expressed Genes That Are Regulators in Cell Cycle Progression ($p < 0.01$)

ID/Transcript	Gene	Description	FC[a]	*p*-value
TC04001516	CCNA2	cyclin A2	-128.34	4.14E-08
TC16000258	PLK1	polo-like kinase 1	-74.07	1.13E-08
TC02002204	BUB1	BUB1 mitotic checkpoint serine/threonine kinase	-66.88	1.73E-07
TC10000373	CDK1	cyclin-dependent kinase 1	-60.17	1.70E-06
TC05000298	CCNB1	cyclin B1	-48.94	2.91E-08
TC01000545	CDC20	cell-division cycle protein 20	-22.46	2.38E-06
TC22000260	MCM5	minichromosome maintenance complex component 5	-21.44	5.51E-08
TC15000449	CCNB2	cyclin B2	-19.92	4.21E-07
TC06001799	MCM3	minichromosome maintenance complex component 3	-18.04	3.59E-08
TC06000761	TTK	TTK protein kinase	-17.66	3.39E-07
TC08000346	MCM4	minichromosome maintenance complex component 4	-16.01	6.10E-08
TC20000968	RBL1	aurora kinase A	-15.67	4.91E-06
TC20000822	9.54	retinoblastoma-like 1	-9.74	9.71E-05
TC17001109	AURKB	aurora kinase B	-8.11	1.08E-05
TC12000496	CDK2	cyclin-dependent kinase 2	-7.32	5.01E-06
TC22000046	CDC45	cell division cycle 45	-6.93	8.09E-07
TC05001829	CDC25C	cell division cycle 25C	-6.33	1.22E-06
TC20000773	E2F1	E2F transcription factor 1	-5.72	1.08E-06
TC03000664	MCM2	minichromosome maintenance complex component 2	-5.26	4.81E-06
TC08001438	CCNE2	cyclin E2	-5	1.70E-05
TC0X001064	SMC1A	structural maintenance of chromosomes 1A	-4.92	8.69E-07
TC01000846	CDC7	cell division cycle 7	-4.82	6.75E-06
TC20000592	PCNA	proliferating cell nuclear antigen	-4.73	9.84E-07
TC07001654	MCM7	minichromosome maintenance complex component 7	-4.04	6.55E-07
TC16000072	CCNF	cyclin F	-3.55	6.73E-06
TC13000426	TFDP1	transcription factor Dp-1	-2.71	2.15E-06
TC08001191	PRKDC	protein kinase, DNA-activated, catalytic polypeptide	-2.68	1.26E-05
TC01000427	HDAC1	histone deacetylase 1	-2.59	3.33E-06
TC15000622	SMAD3	SMAD family member 3	-2.58	2.65E-05
TC20000040	CDC25B	cell division cycle 25B	-2.5	2.05E-06
TC04000176	ANAPC4	anaphase promoting complex subunit 4	-2.43	0.0001
TC12000434	ESPL1	extra spindle pole bodies like 1, separase	-2.23	8.61E-05
TC06001727	CCND3	cyclin D3	-1.61	2.02E-06
TC10000900	BUB3	BUB3 mitotic checkpoint protein	-1.79	1.87E-05
TC12001633	CDK4	cyclin-dependent kinase 4	-1.39	0.0036
TC07001603	CDK6	cyclin-dependent kinase 6	1.24	0.0013

[a]FC, fold changes.

and 1,536 genes were downregulated at a 2-fold or higher level compared to their expression levels in the control. These results are illustrated in a "volcano plot" (Figure 5A) and a heat map generated by hierarchal clustering analysis (Figure 5B). To ease the interpretation of the data, we applied a more stringent cutoff of 5-fold for further analysis. This yielded a subset of 580 genes that were differentially expressed compared to the control. Among the 580 genes that were modulated in response to **3**, 209 were upregulated and 371 were downregulated.

Using Transcriptome Analysis Console (version 4.0.1.36), various biochemical pathways impacted by the >5-fold change in U87 cell gene expression in response to **3** were revealed, which provided further insights into possible mechanisms of its effects. A list of the pathways that were affected is shown in Figure 6. Among the correlated pathways, it was observed that a significant percentage of the genes with greater than 5-fold changes are related to cell cycle and cell proliferation. For example, pathways associated with DNA synthesis, DNA replication, cell cycle, and retinoblastoma protein were almost completely shut down. Conversely, the apoptosis and ferroptosis pathways were more active, with 5 genes and 7 genes being upregulated, respectively. The implications of these findings are discussed below.

Compound 3 Negatively Influences U87 Cell Proliferation, Downregulating CDKs and Shutting down Cell Cycle. The exposure of compound **3** to U87 cells had a significant negative impact on several interconnected biochemical pathways involved in cell cycle and cell growth. The genes associated with cell proliferation that were affected are shown in Table 1, where they are listed in order of decreasing fold change (indicated in the column shaded green). This subset of the gene expression results revealed a global depression of many components of transcriptional function (e.g., the cyclin dependent kinases (CDKs), polo-like kinase 1 (PLK1), and retinoblastoma protein (RBL1)). Furthermore, Aurora and BUB proteins, and the genes responsible for cell division during M phase, were also negatively affected.

Cell cycle is tightly regulated by several protein complexes, and the interactions among them have been studied extensively.[23,24] These complexes are depicted in Figure 7, panel A.[23] Retinoblastoma (RB) protein is a regulatory protein

DOI: 10.1021/acschemneuro.8b00512
ACS Chem. Neurosci. 2019, 10, 1524−1534

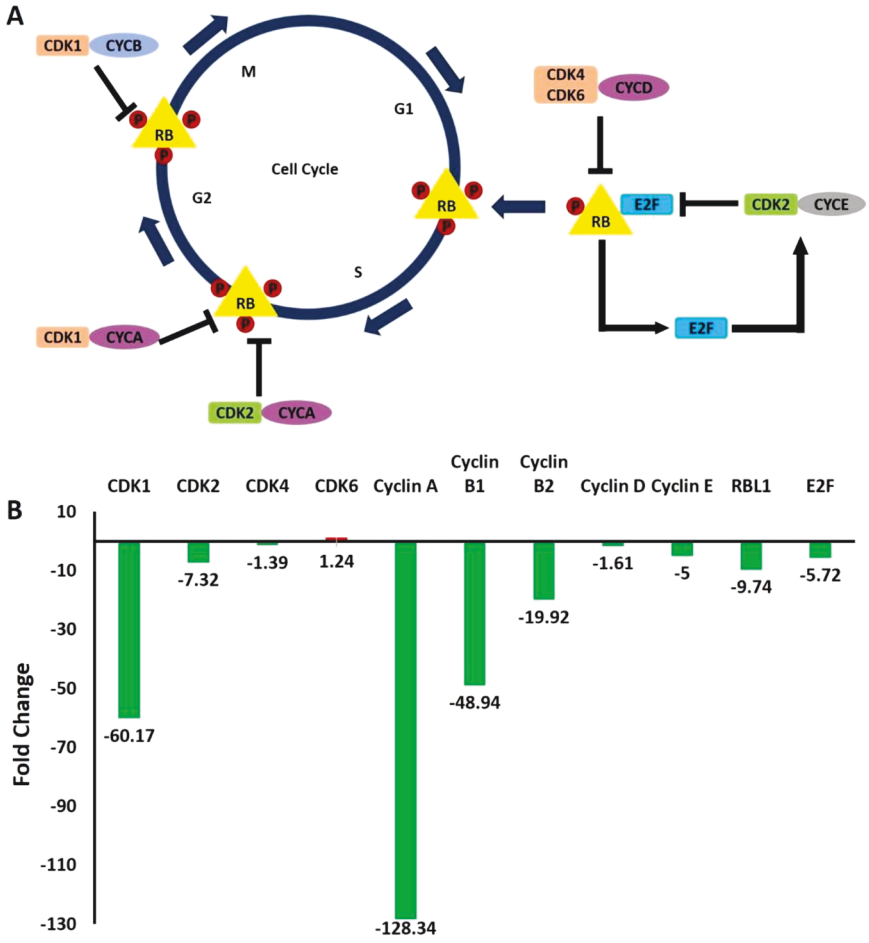

Figure 7. (A) Depiction of the functions of various protein complexes in different stages of cell cycle. (B) Fold changes of the key regulators in cell cycle from the microarray analysis. Green bars indicate downregulation and red bar indicate upregulation ($p < 0.01$).

in this tightly controlled network, and progression through cell cycle requires its phosphorylation.[25,26] When cells in the G0 phase enter into cell cycle, CDK4 (FC: −1.39), CDK6 (FC: 1.24), and the cyclin D (FC: −1.61) protein complexes phosphorylate both RB (FC: −9.74) and E2F (FC: −5.72), and the first phosphorylation event inactivates their repressive function in transcription. Concomitantly, it causes the release of E2F which enters a positive feedback loop that ultimately results in the reinforcement of the phosphorylation of RB. Other complexes in this cascade function in retention of the hyper-phosphorylation of RB. Our microarray results show that CDK1 (FC: −60.17) and CDK2 (FC: −7.32) as well as cyclin A (FC: −128.34) and B (FC: −48.94), which are required to retain the hyper-phosphorylated form of RB, are significantly downregulated. This indicates that the inactivation of the cell cycle suppressor RB is suppressed, possibly resulting in cell cycle being shut down. Furthermore, the proteins that are involved in the initial phosphorylation, CDK2 and cyclin E (FC: −5), are also downregulated, indicating that the synthesis of the hyper-phosphorylated RB is also negatively impacted. The fold changes of these protein complexes are provided in Figure 7B. The results supports the hypothesis that **3** in some way induces interruption of cell cycle by keeping RB from being phosphorylated.

Compound 3 Suppresses the Expression of M Phase Proteins Resulting in Further Negative Impacts on Cell Cycle. Aurora A (AURKA) (FC: −15.67) and PLK1 (FC: −74.07) control the process of the formation of the poles of the mitotic spindle in the early stage of M phase. They were also observed to be downregulated, resulting in an arrest of entry into M phase. The AURKB gene (FC: −8.11), also known as the "equatorial kinase" that is required for cell division, was also observed to be negatively impacted by compound **3**.[27] Additionally, the spindle assembly checkpoint (SAC), which is regulated by a circuit of signaling proteins including budding uninhibited by benzimidazole 1 (BUB1) (FC: −66.88), BUB3 (FC: −1.79), and BUB1B (FC: −9.81) were downregulated. Although defects in SAC are a common characteristic of cancer cells, it has been shown that inhibition of the SAC causes cell death of human cancer cells.[28−30] As shown in our data, BUB1, BUB3, and BUB1B were all downregulated, indicating that the observed cytotoxic effect may also be a consequence of the inhibition of SAC-mediated activities.

qPCR Results Corroborated the Findings of Microarray Experiments. The negative effect of compound **3** on U87 cell cycle was validated by qPCR experiments which were performed to assess the changes in expression of 12 U87 cell cycle genes when the cells were treated at a concentration of 1 mM (48 h post-treatment). Results of the qPCR experiments (presented in Figure 8) showed significant downregulation ($p < 0.005$) of genes that are associated with cell cycle, and these findings were consistent with those observed in the microarray experiments. The influence of compound **3** on cell cycle was

DOI: 10.1021/acschemneuro.8b00512
ACS Chem. Neurosci. 2019, 10, 1524−1534

A

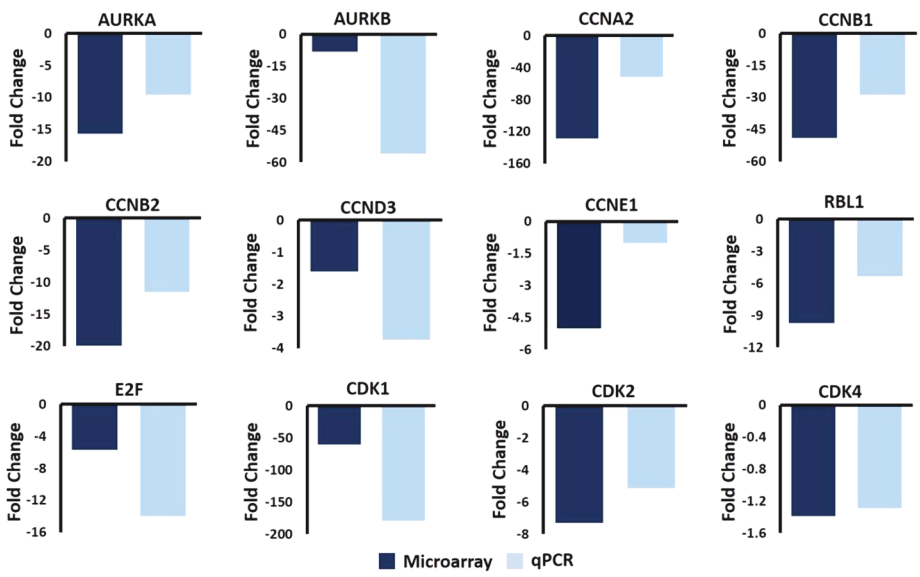

B

Gene symbol	Description	Microarray FC	*p* value	qPCR FC	*p* value
AURKA	Aurora kinase A	-15.67	4.91E-06	-9.58	<1.00E-07
AURKB	Aurora kinase B	-8.11	1.08E-05	-55.83	<1.00E-07
CCNA2	Cyclin A2	-128.33	4.14E-08	-51.86	<1.00E-07
CCNB1	Cyclin B1	-48.94	2.91E-08	-28.87	<1.00E-07
CCNB2	Cyclin B2	-19.92	4.21E-07	-11.55	<1.00E-07
CCND3	CyclinD3	-1.61	2.02E-06	-3.74	1.30E-05
CCNF	Cyclin F	-3.55	6.73E-06	-12.42	<1.00E-07
RBL1	Retinoblastoma-like 1 (p107)	-9.74	9.71E-05	-5.37	<1.00E-07
E2F	E2F transcription factor	-5.72	1.70E-05	-13.98	1.80E-05
CDK1	Cyclin-dependent kinase 1	-60.17	1.70E-06	-179.49	1.00E-06
CDK2	Cyclin-dependent kinase 2	-7.32	5.01E-06	-5.15	<1.00E-07
CDK4	Cyclin-dependent kinase 4	-1.39	3.60E-03	-1.29	<1.00E-07

Figure 8. (A) qRT-PCR validation of differentially expressed U87 genes after 48 h of treatment with compound **3**. Twelve genes were validated using human cell cycle PCR. Gene expression levels are represented as fold changes (*y*-axis). (B) Table displaying the comparison between the microarray and qRT-PCR fold changes.

also confirmed by flow cytometry analysis, which showed that after 48 h, there was a reduction of the cell population in S phase from 14.1% to 5.9%, with increases in cell populations in G0/G1 and G2/M phases of 4% and 4.3%, respectively (Supporting Information Figure S3). The flow cytometry results indicated that entry into S phase is suppressed on exposure to **3**.

The microarray and qPCR findings align with the results of the cell viability studies and shed light on the metabolic impact of the boron-rich delivery agent on cells in the absence of neutron beam treatment. The proteins observed to be suppressed in this study including the polo-like kinase (PLK1), the cyclin-dependent kinases (CDKs), and retinoblastoma protein (RBL1) have been reported to be extensively overexpressed in human cancer due to several genetic mutations that influence the regulatory pathways which ultimately result in uncontrolled proliferation.[2,31−35] We propose that the inhibitory effect of compound **3** on various CDKs and other key regulators in cell cycle limits the progression of U87 cell cycle, and therefore facilitates the induction of apoptotic pathways (5 genes out of 7 exhibited a greater than 5-fold change). These cyclin-dependent kinases have been studied intensively as targets for therapeutic agents against cancer.[36,37] CDK1 in particular, which was down-regulated 60-fold after exposure to compound **3**, is emerging as a potential new target, in addition to the interphase CDKs (CDK2 and CDK4). Because of their important roles in regulating cell cycle, several anticancer agents targeting CDKs are currently being tested in clinical trials.[23]

Although the concentration range in which compound **3** exhibits dramatic effects on U87 cells is relatively high, the distinct gene regulation results observed here suggest new avenues for the application of this and other novel boron delivery agents. For example, the low toxicity of compound **3** at low concentrations makes it possible for it to serve as a short-term local treatment (in the form of an injection, a patch, or infused into gels). By locally administrating the compound, it may be possible to achieve the same dosage (1 mM) in vivo. While the tumor cells are being treated with a relatively high localized concentration of the compound (which then triggers the regulatory effect of the cell cycle genes), the dilution of **3** into the bloodstream may dramatically reduce widespread systemic effects, making the clearance of the agent safer. Importantly, the impact of the carborane motif on cellular gene expression is revealed for the first time, and indicates that the scaffold itself has biological activity independent of that which would be induced by neutron beam irradiation. Although the results presented here may suggest an anticancer effect without the radiation, it would still be informative to explore the effect of the exposure of compound **3** to thermal neutrons. To the

DOI: 10.1021/acschemneuro.8b00512
ACS Chem. Neurosci. 2019, 10, 1524−1534

extent that carborane-containing compounds in and of themselves influence apoptotic and cell-cycle-relevant genes, the cell killing effect of neutron beam radiation may be further amplified, which may be advantageous. The carborane motif is also amenable to the introduction of a broad range of subtle structural modifications, thus enabling the fine-tuning and modulation of its biological properties. In addition to pursing the impact of neutron beam irradiation of cells exposed to **3**, future studies will be focused on assessing whether there is selective uptake of **3** by cancer cells, and on mechanistic investigations of the cellular proteins and organelles that are targeted.

METHODS

Synthesis of 2-Amino-3-(1,7-dicarba-closo-dodecaboranyl-1-thio)propanoic Acid (3). Compound **3** was prepared as previously reported by He et al.[20]

Tissue Culture. The U87 cancer cell line was purchased from ATCC (Manassas, VA). Cells were grown in Eagle Minimum Essential Medium (EMEM) (Invitrogen, Carlsbad, CA) supplemented with 10% FBS and 1 mM sodium pyruvate. Cells were maintained at 37 °C in a humidified environment of 5% CO_2.

Preparation of Media Containing Compound 3. The solid form of compound **3** was added directly in the media which was sonicated until it dissolved. The final concentration was 1 mM. The mixture was then sterile filtered and used directly. For dose response studies, the 1 mM stock solution was diluted to concentrations ranging from 0.1 to 850 μM.

Immunofluorescence Microscopy Imaging. Cells were plated in an 8-well chamber slide system (Thermo Fisher, Waltham, MA) and treated with 1 mM of various *S*-substituted cysteines. The slides were fixed at room temperature in 3% formaldehyde with PBS containing 500 μM Mg^{2+} and 1 mM Ca^{2+} for 10 min, and permeabilized with 0.1% Triton X-100 containing 1% BSA and sodium azide. After washing with PBS, the slides were blocked overnight using PBS with 1% BSA and sodium azide. The cells were stained with AlexaFluoro 488 conjugated Phalloidin (Invitrogen, Carlsbad, CA) for 20 min at room temperature. After washing with PBS, slides were mounted with ProLong Gold Reagent containing DAPI (Invitrogen, Carlsbad, CA). A Leica TCS SP5 Confocal Microscope (Wetzlar, Germany) was used to conduct all imaging studies.

Variable Wavelength Fluorescence Microscopy Imaging. Cultures were inoculated with 4000 cells/chamber, and the U87 cells were grown in EMEM media (500 μL in each chamber) that contained 10% FBS and 1 mM sodium pyruvate at 37 °C for 48 h. After 48 h, the media was replaced with media containing the compound (at a final concentration of 1 mM). Cell morphology changes were monitored at 5 min post-treatment, 24 h post-treatment and 48 h post-treatment. To prepare the media containing the compound, the solid form of the compound was added directly to the media and the solution was sonicated until it dissolved. The final concentration was 1 mM. The mixture was then sterile filtered and used as freshly made. Imaging was performed using a Nikon TE-2000U microscope (Minato, Tokyo, Japan) and Horiba EasyRatiopro X (Horiba Scientific, Edison, NJ) with a scanning range of 250−650 nm. The data were processed using EasyRatioPro Version 2.5 software (Horiba Scientific, Edison, NJ). The imaging was performed in collaboration with Horiba Scientific (Ontario, Canada).

Crystal Violet Assay. U87 cells were inoculated at 12,000 cells/well in 24-well plates for 48 h prior to treatment. Cells were treated with EMEM containing 10% FBS and 1 mM sodium pyruvate with various concentrations of compound **3** for 24 and 48 h. Cells were fixed with 2% glutaraldehyde (Fisher Scientific, Hampton, NH) in PBS for 20 min at room temperature, and then stained with 0.1% crystal violet (Sigma-Aldrich, St. Louis, MO) in DI water for 30 min. After rinsing with water, the plates were dried overnight. The crystal violet stain was solubilized in 0.2% Triton X-100 (Sigma-Aldrich, St. Louis, MO) in distilled water for 30 min with gentle shaking (250 rpm). The absorbance was recorded with a Victor V 1420 Multilabel counter (PerkinElmer Inc., Waltham, MA) at 590 nm. For the control experiments, the same conditions were used and the cells were treated with 1 mM of various *S*-substituted cysteines.

Cell Count Determination. U87 cells were inoculated at 90,000 cells/well in 6-well plates for 40 h prior to treatment. Cells were treated with EMEM containing 10% FBS and 1 mM sodium pyruvate and various *S*-substituted cysteines each at a concentration of 1 mM for 24 and 48 h cell exposure studies. After treatment, the cells were washed with PBS and trypsinized. Muse reagent was added to 25 μL of the cell suspension and the mixture was analyzed using a Muse Cell Analyzer (EMD Millipore, Billerica, MA).

Microarray Analysis. After 48 h, total RNA was isolated from the cells in trizol using a standard protocol followed by cleanup on a RNEasy micro column that included a DNase step. Total RNA (100 ng) was processed using the WT Plus Reagent kit (Affymetrix, Santa Clara, CA). Sense target cDNAs were generated using the standard Affymetrix WT protocol and hybridized to Affymetrix Human Transcriptome 2.0 ST arrays. Arrays were washed, stained and scanned on a GeneChip 3000 7G scanner using Affymetrix GeneChip Command Console Software (AGCC). Transcriptome Analysis Console Software (TAC v4.0.1.36) was used to identify differentially expressed genes. Briefly, the CEL files were summarized using the SST RMA algorithm in TAC and the normalized data were subjected to one-way ANOVA with a Benjamin Hochberg False Discovery Rate correction included ($p < 0.05$). A 2-fold change was used to select entities that were statistically and differentially expressed between the two conditions (treated and untreated). Subsequent identication of significant pathways was restricted to coding genes that were differentially expressed at a 5-fold or higher level.

Human Cell Cycle RT^2 Profiler PCR Arrays. Total RNA was reverse transcribed to cDNA using manufacturer recommendations for the RT^2 First Strand Kit (Qiagen, Germantown, MD). Subsequently qPCR reactions (in a 10 mL reaction volume) using SYBR green Mastermix were set up as recommended for the 384 well human cell cycle RT^2 qPCR arrays (Qiagen, Germantown, MD) on a QuantStudio 12K Flex thermocycler (ThermoFisher, Foster City, CA). Dissociation curve analysis was performed to verify PCR specificity. The results were analyzed using Qiagen RT^2 Profiler PCR Array Data Analysis version 3.5, and fold changes were determined using the $2^{-\Delta Ct}$ method.

Flow Cytometry Experiments. U87 cells were inoculated at 1×10^6 cells/well in 10 cm^2 dish plates for 36 h prior to treatment. Cells were treated with EMEM containing 10% FBS and 1 mM sodium pyruvate with compound **3**, with a final concentration of 1 mM for 36 and 48 h treatments. The cells were then washed with PBS and trypsinized. Muse reagent (EMD Millipore, Billerica, MA) was added to 25 μL of cell suspension and the cell count was determined by Muse Cell Analyzer (EMD Millipore, Billerica, MA). The remaining cell suspension was resuspended in 100 μL PBS and the cells were fixed using 400 μL of 90% ethanol at −20 °C overnight. A cell suspension with ∼300,000 cells was transferred into a tube and 500 μL of PBS containing 0.2% BSA was added. The suspension was spun at 1200 rpm at 4 °C for 3 min. The pellet was washed with 800 μL PBS containing 0.2% BSA and spun down. The pellet was resuspended in 200 μL of Muse cell cycle reagent and incubated for 30 min in the dark at room temperature. The cell suspension was then analyzed using Muse Cell Analyzer (EMD Millipore, Billerica, MA).

ASSOCIATED CONTENT

Supporting Information

The Supporting Information is available free of charge on the ACS Publications website at DOI: 10.1021/acschemneuro.8b00512.

DOI: 10.1021/acschemneuro.8b00512
ACS Chem. Neurosci. 2019, 10, 1524−1534

Variable wavelength fluorescence microscopy imaging results; flow cytometry experiment results of the cells treated with compound **3** after 48 h (PDF)

Accession Codes

Microarray data are deposited in the GEO (Gene Expression Omnibus)[38] database under accession number GSE120066.

AUTHOR INFORMATION

Corresponding Author

*Phone: 518-437-3740. E-mail: rmusah@albany.edu.

ORCID

Rabi A. Musah: 0000-0002-3135-4130

Author Contributions

R.A.M. conceived of the project, performed experiments, and wrote the manuscript with T.H. T.H. performed experiments. S.V.C. oversaw microarray and qPCR experiments and contributed to data interpretation.

Funding

The financial support of the National Science Foundation to R.A.M. (Grants 1310350, 1429329, 0239755, and 1710221) is gratefully acknowledged.

Notes

The authors declare no competing financial interest.

ACKNOWLEDGMENTS

Thanks are extended to Dr. Judy Narvaez for assistance with tissue culture and flow cytometry experiments.

REFERENCES

(1) DeFrancesco, H., Dudley, J., and Coca, A. (2016) Boron chemistry: an overview. In *Boron Reagents in Synthesis*, pp 1−25, American Chemical Society.

(2) Fujimoto, T., Andoh, T., Sudo, T., Fujita, I., Moritake, H., Sugimoto, T., Sakuma, T., Akisue, T., Kawabata, S., Kirihata, M., Suzuki, M., Sakurai, Y., Ono, K., Fukumori, Y., Kurosaka, M., and Ichikawa, H. (2013) Boron neutron capture therapy (BNCT) selectively destroys human clear cell sarcoma in mouse model. *Appl. Radiat. Isot. 73*, 96−100.

(3) Futamura, G., Kawabata, S., Nonoguchi, N., Hiramatsu, R., Toho, T., Tanaka, H., Masunaga, S.-I., Hattori, Y., Kirihata, M., Ono, K., Kuroiwa, T., and Miyatake, S.-I. (2017) Evaluation of a novel sodium borocaptate-containing unnatural amino acid as a boron delivery agent for neutron capture therapy of the F98 rat glioma. *Radiat. Oncol. 12*, 26.

(4) Kueffer, P. J., Maitz, C. A., Khan, A. A., Schuster, S. A., Shlyakhtina, N. I., Jalisatgi, S. S., Brockman, J. D., Nigg, D. W., and Hawthorne, M. F. (2013) Boron neutron capture therapy demonstrated in mice bearing EMT6 tumors following selective delivery of boron by rationally designed liposomes. *Proc. Natl. Acad. Sci. U. S. A. 110*, 6512−6517.

(5) Yokoyama, K., Miyatake, S.-I., Kajimoto, Y., Kawabata, S., Doi, A., Yoshida, T., Asano, T., Kirihata, M., Ono, K., and Kuroiwa, T. (2006) Pharmacokinetic study of BSH and BPA in simultaneous use for BNCT. *J. Neuro-Oncol. 78*, 227−232.

(6) Hattori, Y., Kusaka, S., Mukumoto, M., Uehara, K., Asano, T., Suzuki, M., Masunaga, S.-i., Ono, K., Tanimori, S., and Kirihata, M. (2012) Biological evaluation of dodecaborate-containing amino acids for boron neutron capture therapy. *J. Med. Chem. 55*, 6980−6984.

(7) Barth, R., Coderre, J., Vicente, M., and Blue, T. (2005) Boron neutron capture therapy of cancer: current status and future prospects. *Clin. Cancer Res. 11*, 3987−4002.

(8) Sivaev, I. B., and Bregadze, V. V. (2009) Polyhedral boranes for medical applications: current status and perspectives. *Eur. J. Inorg. Chem. 2009*, 1433−1450.

(9) Hawthorne, M. F., and Lee, M. W. (2003) A critical assessment of boron target compounds for boron neutron capture therapy. *J. Neuro-Oncol. 62*, 33−45.

(10) Henriksson, R., Capala, J., Michanek, A., Lindahl, S.-Å., Salford, L. G., Franzén, L., Blomquist, E., Westlin, J.-E., and Bergenheim, A. T. (2008) Boron neutron capture therapy (BNCT) for glioblastoma multiforme: A phase II study evaluating a prolonged high-dose of boronophenylalanine (BPA). *Radiother. Oncol. 88*, 183−191.

(11) Hopewell, J. W., Gorlia, T., Pellettieri, L., Giusti, V., H-Stenstam, B., and Sköld, K. (2011) Boron neutron capture therapy for newly diagnosed glioblastoma multiforme: An assessment of clinical potential. *Appl. Radiat. Isot. 69*, 1737−1740.

(12) Kankaanranta, L., Seppälä, T., Koivunoro, H., Saarilahti, K., Atula, T., Collan, J., Salli, E., Kortesniemi, M., Uusi-Simola, J., Välimäki, P., Mäkitie, A., Seppänen, M., Minn, H., Revitzer, H., Kouri, M., Kotiluoto, P., Seren, T., Auterinen, I., Savolainen, S., and Joensuu, H. (2012) Boron neutron capture therapy in the treatment of locally recurred head-and-neck cancer: final analysis of a phase I/II trial. *Int. J. Radiat. Oncol., Biol., Phys. 82*, e67−e75.

(13) Nakai, K., Yamamoto, T., Aiyama, H., Takada, T., Yoshida, F., Kageji, T., Kumada, H., Isobe, T., Endo, K., Matsuda, M., Tsurubuchi, T., Shibata, Y., Takano, S., Mizumoto, M., Tsuboi, K., and Matsumura, A. (2011) Boron neutron capture therapy combined with fractionated photon irradiation for glioblastoma: A recursive partitioning analysis of BNCT patients. *Appl. Radiat. Isot. 69*, 1790−1792.

(14) Valliant, J. F., Guenther, K. J., King, A. S., Morel, P., Schaffer, P., Sogbein, O. O., and Stephenson, K. A. (2002) The medicinal chemistry of carboranes. *Coord. Chem. Rev. 232*, 173−230.

(15) Hawthorne, M. F. (1993) The role of chemistry in the development of boron neutron capture therapy of cancer. *Angew. Chem., Int. Ed. Engl. 32*, 950−984.

(16) Hawthorne, M. F. (1998) New horizons for therapy based on the boron neutron capture reaction. *Mol. Med. Today 4*, 174−181.

(17) Soloway, A. H., Tjarks, W., Barnum, B. A., Rong, F.-G., Barth, R. F., Codogni, I. M., and Wilson, J. G. (1998) The chemistry of neutron capture therapy. *Chem. Rev. 98*, 2389−2390.

(18) Goodman, J. H., Yang, W., Barth, R. F., Gao, Z., Boesel, C. P., Staubus, A. E., Gupta, N., Gahbauer, R. A., Adams, D. M., Gibson, C. R., Ferketich, A. K., Moeschberger, M. L., Soloway, A. H., Carpenter, D. E., Albertson, B. J., Bauer, W. F., Zhang, M. Z., and Wang, C. C. (2000) Boron neutron capture therapy of brain tumors: biodistribution, pharmacokinetics, and radiation dosimetry of sodium borocaptate in patients with gliomas. *J. Neurosurg. 47*, 608−622.

(19) Koivunoro, H., Hippeläinen, E., Auterinen, I., Kankaanranta, L., Kulvik, M., Laakso, J., Seppälä, T., Savolainen, S., and Joensuu, H. (2015) Biokinetic analysis of tissue boron (^{10}B) concentrations of glioma patients treated with BNCT in Finland. *Appl. Radiat. Isot. 106*, 189−194.

(20) He, T., Misuraca, J. C., and Musah, R. A. (2017) Carboranyl-cysteine"—synthesis, structure and self-assembly behavior of a novel α-amino acid. *Sci. Rep. 7*, 16995.

(21) Sauerwein, W. (1997) Considerations about specifications and reporting of dose in BNCT. In *Advances in Neutron Capture Therapy* (Larsson, B., Crawford, J., and Weinreich, R., Eds.), pp 531−534, Excerpta Medica.

(22) Gabel, D., Foster, S., and Fairchild, R. G. (1987) The monte carlo simulation of the biological effect of the ^{10}B (n,α) ^{7}Li reaction in cells and tissue and its implication for boron neutron capture therapy. *Radiat. Res. 111*, 14−25.

(23) Lapenna, S., and Giordano, A. (2009) Cell cycle kinases as therapeutic targets for cancer. *Nat. Rev. Drug Discovery 8*, 547.

(24) Malumbres, M., and Barbacid, M. (2009) Cell cycle, CDKs and cancer: a changing paradigm. *Nat. Rev. Cancer 9*, 153.

(25) Giacinti, C., and Giordano, A. (2006) RB and cell cycle progression. *Oncogene 25*, 5220.

(26) Weinberg, R. A. (1995) The retinoblastoma protein and cell cycle control. *Cell 81*, 323−330.

DOI: 10.1021/acschemneuro.8b00512
ACS Chem. Neurosci. 2019, 10, 1524−1534

(27) Barr, A. R., and Gergely, F. (2007) Aurora-A: the maker and breaker of spindle poles. *J. Cell Sci. 120*, 2987−2996.
(28) Kops, G. J. P. L., Foltz, D. R., and Cleveland, D. W. (2004) Lethality to human cancer cells through massive chromosome loss by inhibition of the mitotic checkpoint. *Proc. Natl. Acad. Sci. U. S. A. 101*, 8699−8704.
(29) Kops, G. J. P. L., Weaver, B. A. A., and Cleveland, D. W. (2005) On the road to cancer: aneuploidy and the mitotic checkpoint. *Nat. Rev. Cancer 5*, 773.
(30) Weaver, B. A. A., Silk, A. D., and Cleveland, D. W. (2008) Low rates of aneuploidy promote tumorigenesis while high rates of aneuploidy cause cell death and tumor suppression. *Cell. Oncol. 30*, 453−453.
(31) Liu, X., and Erikson, R. L. (2003) Polo-like kinase (Plk)1 depletion induces apoptosis in cancer cells. *Proc. Natl. Acad. Sci. U. S. A. 100*, 5789−5794.
(32) Malumbres, M., and Barbacid, M. (2001) Milestones in cell division: To cycle or not to cycle: a critical decision in cancer. *Nat. Rev. Cancer 1*, 222.
(33) Malumbres, M., and Barbacid, M. (2005) Mammalian cyclin-dependent kinases. *Trends Biochem. Sci. 30*, 630−641.
(34) Malumbres, M., and Barbacid, M. (2007) Cell cycle kinases in cancer. *Curr. Opin. Genet. Dev. 17*, 60−65.
(35) Paggi, M. G., and Giordano, A. (2001) Who is the boss in the retinoblastoma family? The point of view of Rb2/p130, the little brother. *Cancer Res. 61*, 4651−4654.
(36) Shapiro, G. I. (2006) Cyclin-dependent kinase pathways as targets for cancer treatment. *J. Clin. Oncol. 24*, 1770−1783.
(37) Enserink, J. M., and Kolodner, R. D. (2010) An overview of Cdk1-controlled targets and processes. *Cell Div. 5*, 11.
(38) Edgar, R., Domrachev, M., and Lash, A. E. (2002) Gene expression omnibus: NCBI gene expression and hybridization array data repository. *Nucleic Acids Res. 30*, 207−210.

DOI: 10.1021/acschemneuro.8b00512
ACS Chem. Neurosci. 2019, 10, 1524−1534